



OPEN ACCESS

EDITED BY

Venkaiah Betapudi,
United States Department of Health and
Human Services, United States

REVIEWED BY

Dipak Maskey,
Henry Ford Health System,
United States
Yutaro Komuro,
UCLA, United States

*CORRESPONDENCE

Diana Valverde,
dianaval@uvigo.es

SPECIALTY SECTION

This article was submitted to Cellular
Biochemistry,
a section of the journal
Frontiers in Molecular Biosciences

RECEIVED 12 July 2022

ACCEPTED 13 September 2022

PUBLISHED 13 October 2022

CITATION

Bea-Mascato B, Neira-Goyanes E,
Iglesias-Rodríguez A and Valverde D
(2022), Depletion of *ALMS1* affects TGF- β
signalling pathway and downstream
processes such as cell migration and
adhesion capacity.
Front. Mol. Biosci. 9:992313.
doi: 10.3389/fmolb.2022.992313

COPYRIGHT

© 2022 Bea-Mascato, Neira-Goyanes,
Iglesias-Rodríguez and Valverde. This is
an open-access article distributed
under the terms of the [Creative
Commons Attribution License \(CC BY\)](#).
The use, distribution or reproduction in
other forums is permitted, provided the
original author(s) and the copyright
owner(s) are credited and that the
original publication in this journal is
cited, in accordance with accepted
academic practice. No use, distribution
or reproduction is permitted which does
not comply with these terms.

Depletion of *ALMS1* affects TGF- β signalling pathway and downstream processes such as cell migration and adhesion capacity

Brais Bea-Mascato^{1,2}, Elena Neira-Goyanes^{1,2},
Antía Iglesias-Rodríguez^{1,2} and Diana Valverde^{1,2*}

¹CINBIO, Universidad de Vigo, Vigo, Spain, ²Grupo de Investigación en Enfermedades Raras y Medicina Pediátrica, Instituto de Investigación Sanitaria Galicia Sur (IIS Galicia Sur), SERGAS-UVIGO, Vigo, Spain

Background: *ALMS1* is a ubiquitous gene associated with Alström syndrome (ALMS). The main symptoms of ALMS affect multiple organs and tissues, generating at last, multi-organic fibrosis in the lungs, kidneys and liver. TGF- β is one of the main pathways implicated in fibrosis, controlling the cell cycle, apoptosis, cell migration, cell adhesion and epithelial-mesenchymal transition (EMT). Nevertheless, the role of *ALMS1* gene in fibrosis generation and other implicated processes such as cell migration or cell adhesion *via* the TGF- β pathway has not been elucidated yet.

Methods: Initially, we evaluated how depletion of *ALMS1* affects different processes like apoptosis, cell cycle and mitochondrial activity in HeLa cells. Then, we performed proteomic profiling with TGF- β stimuli in HeLa *ALMS1* $-/-$ cells and validated the results by examining different EMT biomarkers using qPCR. The expression of these EMT biomarkers were also studied in hTERT-BJ-5ta *ALMS1* $-/-$. Finally, we evaluated the SMAD3 and SMAD2 phosphorylation and cell migration capacity in both models.

Results: Depletion of *ALMS1* generated apoptosis resistance to thapsigargin (THAP) and C2-Ceramide (C2-C), and G2/M cell cycle arrest in HeLa cells. For mitochondrial activity, results did not show significant differences between *ALMS1* $+/+$ and *ALMS1* $-/-$. Proteomic results showed inhibition of downstream pathways regulated by TGF- β . The protein-coding genes (PCG) were associated with processes like focal adhesion or cell-substrate adherens junction in HeLa. *SNAI1* showed an opposite pattern to what would be expected when activating the EMT in HeLa and BJ-5ta. Finally, in BJ-5ta model a reduced activation of SMAD3 but not SMAD2 were also observed. In HeLa model no alterations in the canonical TGF- β pathway were observed but both cell lines showed a reduction in migration capacity.

Conclusion: *ALMS1* has a role in controlling the cell cycle and the apoptosis processes. Moreover, the depletion of *ALMS1* affects the signal transduction through the TGF- β and other processes like the cell migration and adhesion capacity.

KEYWORDS

ALMS1, alström syndrome, ciliopathies, primary cilia, TGF- β , epithelial-mesenchymal transition (EMT), cell cycle arrest, apoptosis

Introduction

ALMS1 is a ubiquitous gene with 23 exons located on chromosome 2p13. Mutations in this gene are related to Alström syndrome (ALMS; OMIM #203800), a rare, autosomal and recessive disease with a prevalence of 1–9 cases per 1,000,000 inhabitants and approximately 950 cases reported worldwide (Orphanet). The main symptoms of ALMS affect multiple organs and tissues (Marshall et al., 2011), such as cone-rod retinal dystrophy, dilated cardiomyopathy (DCM) and hypertension (Jaykumar et al., 2017), hypertriglyceridemia, type II diabetes mellitus (T2D) (Collin et al., 2002), and hepatic, renal and pulmonary dysfunction caused by multi-organ fibrosis (Marshall et al., 2007; Marshall et al., 2011), which is the main cause of death in these patients.

The protein encoded by *ALMS1* plays a structural role in the eukaryotic cell centrosomes (Hearn et al., 2005), a microtubule (MT)-nucleating organelle strongly related to primary cilia. The *ALMS1* basal body location (Hearn et al., 2005; Jagger et al., 2011) has been related to different functions controlled by the primary cilium such as centrosome cohesion, cell cycle control and endosomal trafficking (Li et al., 2007; Jagger et al., 2011; Zulato et al., 2011; Leitch et al., 2014).

Although numerous roles of *ALMS1* have been described at both ciliary and extraciliary levels, the regulation of the pathways underlying these cellular processes remain unknown. Recently, our group has established the relationship between the *ALMS1* gene and the TGF- β signaling pathway (Álvarez-Satta et al., 2021), which could be related to the development of fibrosis in these patients (Roberts et al., 2006; Walton et al., 2017). TGF- β is a signalling pathway regulated by clathrin-dependent endocytosis (CDE) in the pocket region of primary cilium (Clement et al., 2013), and coordinates cell cycle, apoptosis and migration processes such as epithelial-mesenchymal transition (EMT) (Zhang et al., 2017). This pathway acts in close coordination with other signalling cascades such as Wnt, Hippo, Notch, Hedgehog (Hh), mitogen-activated protein kinase (MAPK), and phosphoinositide 3-kinase (PI3K)-Akt, resulting in many cases in complex regulatory networks dependent on the primary cilium (Luo, 2017).

Stimulation of the TGF- β pathway can activate two main cascades: The canonical (SMAD-dependent) pathway and the non-canonical (SMAD-independent) pathway (Massagué, 2012). The canonical pathway is coordinated by transcription factors called R-SMAD (SMAD2 and SMAD3) which join co-SMAD (SMAD4) to activate the expression of several genes such as *SNAI1* (Nakao et al., 1997; Thuault et al., 2008), a key modulator of EMT (Vincent et al., 2009; Wang et al., 2013). This pathway is inhibited by an I-SMAD, SMAD7, which inhibits R-SMAD signalling in a variety of ways, binding to TGF- β receptors or

directly in the nucleus, avoiding the binding of the R-Smad-Smad4 complex to DNA (Yan et al., 2016). On the other hand, the non-canonical activation pathway includes a wide group of pathways such as p38 MAPK, PI3K/AKT, or Rho GTPases (Massagué, 2012). Recently, studies have linked the abolition of several centrosomal proteins such as *ALMS1* and *CEP128* to the inhibition of the SMAD-dependent canonical pathway in zebrafish and various human cell types such as hTERT-RPE1 and ciliated human foreskin fibroblasts (hFF) (Mönnich et al., 2018; Álvarez-Satta et al., 2021). However, deciphering how centrosomal proteins coordinate and regulate the TGF- β signalling pathway and their downstream processes is a challenge.

Determining how *ALMS1* regulates cell migration and adhesion processes such as EMT is critical to understanding how multi-organ fibrosis occurs in Alström syndrome. In this article, we analysed how the lack of *ALMS1* could affect different cell processes such as mitochondrial activity, cell cycle, apoptosis, and signal transduction through the TGF- β pathway. Moreover, we evaluated the expression pattern for different EMT biomarkers after TGF- β pathway stimulation in two independent CRISPR-KO cell models (HeLa and BJ-5ta) for *ALMS1*. Finally, we measured p-SMAD3 and p-SMAD2 activation and migration capacity in the presence and absence of the TGF- β 1 ligand.

Materials and methods

Cell culture

HeLa human cervical cancer cell line from American Type Culture Collection (ATCC), hTERT BJ-5ta human dermal fibroblasts (ATCC) and 293T human embryonic kidney cell line from ATCC were used in this study. HeLa and 293T cells were maintained in Dulbecco's minimum essential medium (DMEM, Gibco, Invitrogen, NY, United States), supplemented with 10% fetal bovine serum (FBS) (Gibco, Invitrogen, NY, United States) and 2% penicillin/streptomycin (P/S) (Gibco, Invitrogen, NY, United States). In the case of BJ-5ta line, cells were maintained in DMEM:199, supplemented with 10% of FBS, 2% P/S and Hygromycin B (0.01 mg/ml). All cell lines were grown at 37°C with 5% CO₂ for up to 1 month. After this, the cells were discarded, and a new culture was started.

Criscpr assay and edition validation

HeLa cells were edited with a dual episomal system for homology directed repair (HDR) (Santa Cruz Biotechnology,

Inc., Dallas, United States). Cells were transfected with Lipofectamine 2000 (Thermo Fisher, Waltham, United States) with 3 gRNAs directed to *ALMS1* exons 1 and 3 (Supplementary Table S1) following the manufacturer's protocol. After plasmid transfection, cells were selected with puromycin (1 µg/ml) for 5 days (Supplementary Figure S1).

BJ-5ta cells were edited using a lentivirus system according to the protocol described by Sanjana et al. (2014), with some modifications. Check Supplementary Material for more information. After lentiviral transduction, cells were selected with puromycin (1 µg/ml) for 5 days (Supplementary Figure S2).

Surviving cells were expanded and isolated to obtain individual clones. Of the isolation was performed using Fluorescence-Activated Cell Sorting (FACS) with Hoechst (BD Bioscience, San José, United States) in the flow cytometer FACS ARIA III (BD Bioscience, San José, United States). Inhibition of gene expression was validated by qPCR in a StepOnePlus instrument (Thermo Fisher, Waltham, United States). A commercial probe TaqMan® Gene Expression Assays (Hs00367316_m1) and PrimeTime® qPCR Primer Assays (Hs.PT.56a.488948) were used to detect *ALMS1* in the HeLa and BJ-5ta models, respectively.

Mitochondrial activity assay

Mitochondrial activity was evaluated using Presto Blue reagent (Thermo Fisher, Waltham, United States). Wild type (*ALMS1* +/+; WT) and HeLa Knockout cells (*ALMS1* -/-; KO) were seeded in 96-well plates by triplicate in concentrations from 5×10^4 to 1.5×10^3 cells per well. The plates were incubated for 24 h as previously described. After incubation, 10 µL of Presto Blue were added to each well and cells were incubated for 2 h. Next, the plate was centrifuged at 1500 rpm for 5 min and the supernatant was transferred to a fluorescence plate (Corning, NY, United States). Finally, the plates were measured in the Envision plate reader (Perkin-Elmer, Waltham, United States). This experiment was repeated 3 times on different days.

Apoptosis assay

The apoptosis assay was performed in flat-bottom 96-well plates. HeLa *ALMS1* +/+ and *ALMS1* -/- cells were seeded in triplicate at a concentration of 3×10^4 cells/per well and incubated 24 h in DMEM 2%P/S and 2%FBS before treatment. Next, apoptotic stimuli were added at final concentration of 100 nM for thapsigargin (THAP) and 25 µM for C2-ceramide (C2-C) in plates, followed by incubation at 37°C for 24–48 h respectively. After that, cells were washed twice with 100 µL PBS. 50 µL trypsin was added per well and the plate was incubated for 5 min at 37°C. After that, trypsin was inactivated with 50 µL DMEM 10% FBS 2% P/S, and cells were transferred to

96-well plates with U bottom. The plate was centrifuged at 1500 rpm for 5 min, the supernatant was discarded, and the cells were resuspended in 200 µL binding buffer with 2 µL 7-AAD and 2 µL annexin V-FITC (Biolegend Inc., San Diego, CA, United States). The plate was incubated for 15 min in darkness and measured in the flow cytometer FC 500 (Beckman-Coulter, Brea, CA, United States). This experiment was repeated 3 times on different days.

Cell cycle assay

To determine cell cycle alterations, we studied subpopulations in the HeLa *ALMS1* -/- model with Hoechst staining (BD Bioscience, San José, United States). *ALMS1* +/+ and *ALMS1* -/- cells were seeded in a 6-well plate at a concentration of 3×10^5 cells/per well and incubated overnight. The next day, 1 µL Hoechst staining was added to the medium and the plate was incubated for 1 h. Then, the medium was removed, cells were washed twice with 1 ml PBS per well, and trypsinised following the protocol described above. Cells were resuspended in PBS and analysed in the flow cytometer FACS ARIA III.

Protein extraction for proteomic profiling

HeLa cells were seeded in 6-well plates by triplicate in DMEM 2% P/S, 2%FBS and incubated overnight for serum starvation. One the next day, cells were stimulated with rhTGF-β1 (2 ng/ml; R&D Systems; 240-B) for 24 h. After that, DMEM was removed, and wells were washed twice with PBS. Cells were scrapped in PBS. Then, cells were pelleted at 11000 rpm for 5 min, and 100 µL of RIPA Buffer were added to each sample. Samples were incubated on ice for 20 min in constant agitation. Finally, cell debris was pelleted by centrifugation for 30 min at 12000 rpm and 4°C. Samples were aliquoted and stored at -80°C until the next protocol's step. Protein quantification was performed by Bradford microplate assay (Bio-Rad, Hercules, United States).

Protein concentration, reduction and alkylation

Initially, 20 µg of each sample was concentrated and stained with Coomassie in a 12% SDS-PAGE gel. Bands were cut and faded. Band distinction was performed by adding 100 µL of ammonium bicarbonate 25 mM/50% acetonitrile and incubated 20 min. This step was repeated 4 times. After distinction, the supernatant was removed and 100 µL of ammonium bicarbonate 25 mM-50% EtOH was added to samples, and incubated for 20 min. Then, the supernatant was

removed and 100 μ L EtOH was added and incubated for 15 min. In the next step, 200 μ L 10 mM DTT in ammonium bicarbonate were added and samples were incubated for 1 h at 56°C. Then, DTT solution was removed and 200 μ L iodoacetamide (IAA) 55 mM in 50 mM ammonium bicarbonate was added. Samples were incubated again for 30 min at room temperature. Finally, the supernatant was removed, 200 μ L ammonium bicarbonate 50 mM were added and samples were incubated for 15 min.

Protein digestion

After reduction and alkylation, samples were digested. 100 μ L ammonium bicarbonate 25 mM-50% acetonitrile (ACN) was added to each sample and incubated for 30 min. The supernatant was removed and 100 μ L ACN 100% was added and incubated for 10 min. The supernatant was removed again and 15 μ L Trypsin in ammonium bicarbonate 25 mM were added to each sample. Samples were maintained at 4°C for 30 min. Finally, trypsin was removed, 5 μ L ammonium bicarbonate 25 mM were added, and samples were incubated overnight.

Peptide extraction

40 μ L of trifluoroacetic acid (TFA) 0.5% were added to each sample and incubated for 30 min at room temperature. Then, we added 20 μ L ACN 100% in each 1.5 ml tube and incubated for 15 min at 37°C. Finally, the samples were dried in a speed-vac at 45°C for 1 h and stored at -20°C until the analysis.

Mass spectrometry and bioinformatic analysis

Samples were resuspended in 24 μ L formic acid 0.1%. Then, 10 μ L were injected into the HPLC (LC-ESI-MS/MS workflow using a C18 precolumn). Samples were analysed in a mass spectrophotometry Orbitrap ELITE (Thermo-Fisher, Waltham, United States) in long chromatography mode (4 h). After that, protein identification was performed in the database UniProtKB/TrEMBL for humans, using the Proteome Discoverer software (v2.1) (Supplementary Table S2). Downstream analysis was performed with the R package Differential Enrichment analysis of Proteomics data (DEP package) (Zhang et al., 2018). Finally, Go Terms analysis was performed with ClusterProfiler package (Yu et al., 2012), and results were visualized with GPlot package (Walter et al., 2015). All the code for the analysis was deposited in the GitHub repository (https://github.com/BreisOne/CRISPR_HeLa_KO_Alms1).

The mass spectrometry proteomics data have been deposited in the ProteomeXchange Consortium via the PRIDE (Perez-

Riverol et al., 2019) partner repository with the dataset identifier PXD024964.

RNA extraction and RT-PCR

HeLa cells were seeded in 6-well plates at a concentration of 2×10^5 by triplicate in DMEM 2%P/S and 2%FBS and were incubated overnight for serum starvation. The next day, cells were stimulated with rhTGF- β 1 (2 ng/ml) for 24, 48 and 72 h. DMEM was removed and wells were washed twice with PBS. Cells were scraped in PBS and collected in a 1.5 ml tubes. For the RNA extraction, the NYZ total RNA isolation kit (NYZtech, Lisboa, Portugal) was used following the manufacture's protocol.

After RNA elution, the sample concentrations were measured with Nanodrop (Thermo Fisher, Waltham, United States). Next, 300 ng of RNA were retrotranscribed to cDNA using the NZY First-Strand cDNA Synthesis kit (NYZtech, Lisboa, Portugal) following the manufacture's protocol.

For the experiment with the BJ-5ta line, the same protocol was followed but using DMEM:199 and stimulating for 24 and 48 h only.

qPCR expression analysis

Samples were prepared in 96-well plates (Thermo Fisher, Waltham, United States) adding 1 μ L of each primer, 12.5 μ L of PowerUp SYBR Green Master Mix (Thermo Fisher, Waltham, United States), 1 μ L of cDNA and 4.5 μ L of H₂O_d in a final volume of 20 μ L per well. qPCRs were performed in StepOnePlus instrument using the following, cycling conditions: 10 min at 95°C, 40 cycles of 15 s at 95°C and 1 min at 60°C. Primers were synthesized on demand (IDT) (Supplementary Table S3). Samples were analysed by technical triplicates for each sample and gene. Cts for technical triplicates were averaged using the geometric mean and $\Delta\Delta$ CT method was applied for the normalization, using 2 housekeeping (HK) genes (*ALAS1* and *YWHAZ*).

Wound healing assay

BJ-5ta and HeLa (WT and KO) were seeded in a 24-well plate (6 wells per cell line and genotype) at a concentration of 1×10^5 and cultured until a 90–95% of confluence. Cells were serum-starvated (2%FBS for HeLa cells) for 24 h. After that, rh-TGF- β 1 (2 ng/ml) was added to half of the wells and a wound performed with a 200 μ L pipette tip. Cells were incubated at 37°C 5% CO₂ and images were taken at 0 and 24 h with the microscope inverted Nikon TiU. Images were analysed with the ImageJ program (Schneider et al., 2012) and the plugin developed by

Suarez-Armendo et al. (2020). Finally, the percentage of closure was measured with respect to the wound area at time 0 h.

SMADs activation assays

For p-SMADs/SMADs activation assays, BJ-5ta and HeLa (WT and KO) cells were plated in 100 mm dishes (Corning, NY, United States) and incubated in DMEM:199 2P/S% without FBS and DMEM 2% P/S, 2%FBS for 24 h, respectively. Then, TGF- β pathway were stimulated adding rhTGF- β 1 ligand at 2 ng/ml (final concentration in dish) for 0, 10, 30, and 90 min in BJ-5ta and 0 and 30 min in HeLa. After stimulation, cells were washed 3 times with PBS, harvested using a scraper, and centrifuged in a Sigma[®] 1–14 K at 4°C, 7,400 \times g for 10 min. Then, pellets were lysed on ice for 10 min in 200 μ L of RIPA lysis buffer containing 1 mM sodium orthovanadate as phosphatase inhibitor (Sigma-Aldrich, Misuri, United States) and 0.1% (v/v) protease inhibitor cocktail (Merck, Darmstadt, Germany). Lysates were centrifuged at 4°C, 14,500 \times g for 30 min, and the supernatant was collected in 1.5 ml low binding tubes (Thermo Fisher, Waltham, United States). The remaining pellet was discarded. Quantification was performed using Bradford assay in microplates with Bio-Rad protein assay and samples were stored at –80°C until analysis.

SDS-PAGE, Western Blotting, and quantification

A total amount of 20 μ g from each sample were mixed with 6,25 μ L of Laemmli Buffer 4X (Biorad, Hercules, United States), 1,25 μ L β -mercaptoethanol (BME) and a volume of H₂O_d up to a final volume of 25 μ L. Then, the mixes were boiled at 97°C for 5 min and loaded in a Mini-PROTEAN[®] TGX[™] Precast Gel (Biorad, Hercules, United States) at 12% acrylamide/bis-acrylamide. The gel was migrated for 1 h at 150 V. Then, gels were transferred to a 0.2 μ m PVDF membrane using the Trans-Blot Turbo transfer system (Biorad, Hercules, United States) following the mixed molecular weight (MW) protocol. After transfer, membranes were blocked with in-house tris-buffered saline, 0.1% Tween20 and 5% milk (TBS-T 5%) for 90 min. Incubation with the primary antibody was kept at 4°C overnight. The primary antibodies used in this assay were: anti-SMAD3 (1:1000, Abcam, 40854), anti-p-SMAD3 (1:1000, Abcam, 63403), anti-SMAD2 (1:1000, Abcam, 40855), anti p-SMAD2 (1:1000, Cell Signaling Technology, 3101).

Next day, incubation with secondary antibody was performed by 45 min in TBST 5%, after washed the membrane 3 times in TBST 5%. The secondary antibody used in this assay was goat anti-rabbit IgG H&L (HRP) (Abcam, 205718) at 1:5000 for p-SMAD2 and p-SMAD3 and 1:15000 for SMAD2 and SMAD3. Finally, for protein visualization Clarity

western ECL substrate (Biorad, Hercules, United States) was used and membranes were exposed in the ChemiDoc system (Biorad, Hercules, United States). Quantification of protein bands was carried on Image Lab software (Biorad, Hercules, United States) using the total protein standardisation method.

Western Blotting membranes were stripped and re-probed using Restore[™] PLUS Western Blot Stripping Buffer (Thermo Fisher, Waltham, United States) according to the manufacturer's protocol. Incubation for 15 min in the buffer was followed by 3 washes with 1X TBS. Then, the membranes were re-blocked and re-labelled following the previously described protocol.

Statistical analysis

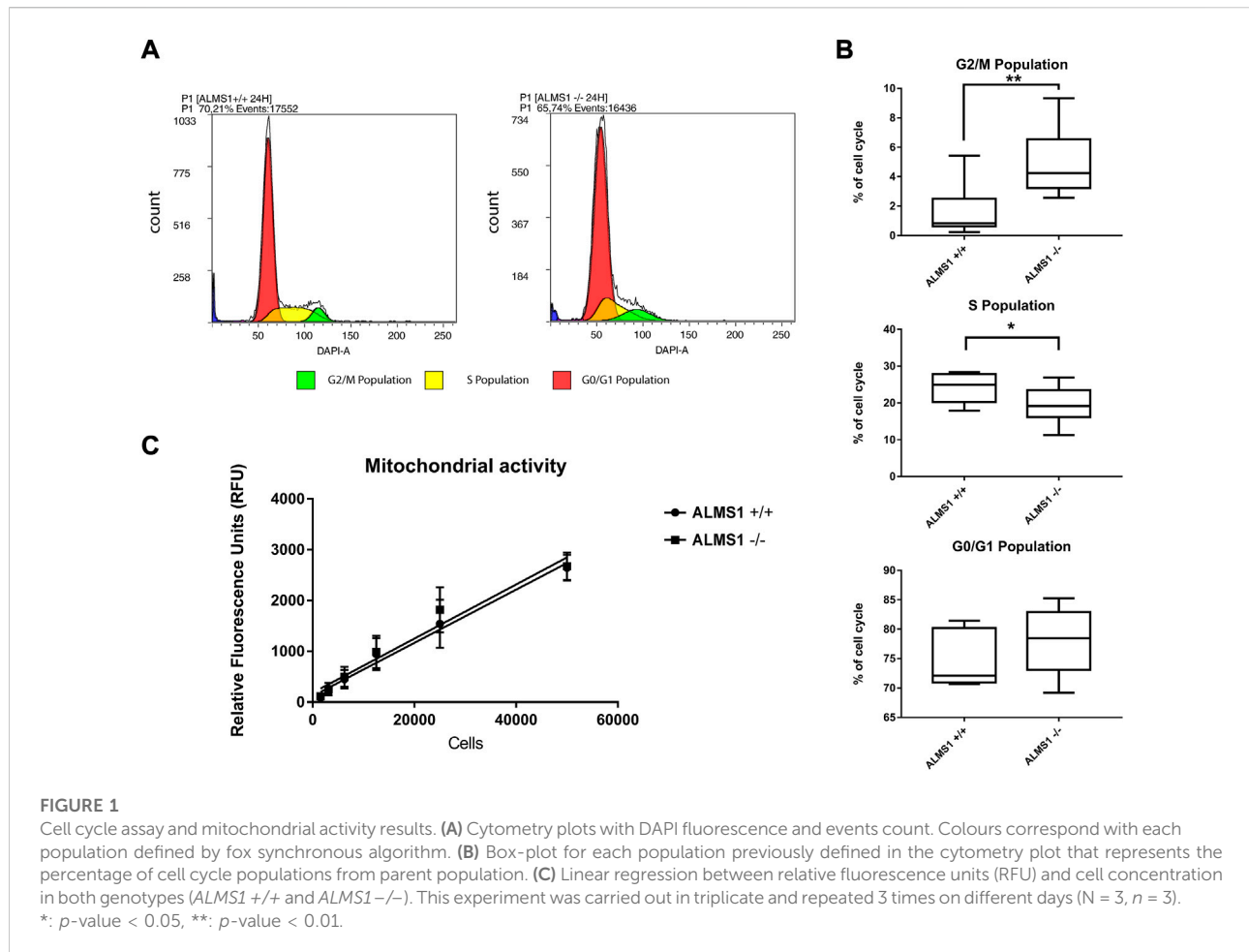
On one hand, mitochondrial activity, apoptosis, cell cycle, qPCR, Western Blot and wound healing data visualization and statistical analysis were performed with the software GraphPad Prism 8.00.

Mitochondrial activity was analysed using a linear regression model. Comparison of fluorescence increase with cell concentration did not show significant differences between both slopes ($\alpha = 0.05$). The apoptosis experiment results were analysed with 2ways-Anova to compare each different population between genotypes. A Sidak's multiple comparisons test was applied to correct the analysis. Finally, cell cycle results were analysed with a two-tailed unpaired *t*-test for each population (G2/M, S and G0/G1).

On the other hand, proteomic data analysis included different statistical analyses and data transformations along the pipeline. Initially, the data were normalised by variance stabilizing transformation (VSN). The data imputation for missing values was performed like missing not at random (MNAR) using the Minprob method with FDR <0.01. Finally, differential expression analysis was performed using protein-wise linear models combined with empirical Bayes statistics implemented in the limma package, FDR <0.05.

A third analysis was performed for the qPCR data. After normalization, fold changes (FC) were calculated concerning the geometric mean of the expression of each gene in the biological triplicates for *ALMS1* +/+ at 24 h. Significant differences were calculates using a multiple *t*-test with a significant threshold of FDR <0.05.

Finally western-blot data were normalized using total protein method following the methodology used by Clement et al. (2013); Mönnich et al., 2018) and as modified by Gürtler et al. (2013). After normalization FCs were calculated respect WT at 30 min of TGF- β 1 stimulation. Significant differences were calculates using 2-way-ANOVA with a significant threshold of adj. *p*-value (FDR) < 0.05. For wound healing assay, an 2-way-ANOVA was applied and a significant threshold of adj. *p*-value (FDR) < 0.05 was set.



Results

ALMS1 depletion does not alter mitochondrial basal activity despite generating G2/M cell cycle arrest in HeLa cells

ALMS1 is a structural centromere protein (Hearn et al., 2005) that controls the structure of the cytoskeleton (Collin et al., 2012). Since *ALMS1* depletion causes cell cycle elongation (Zulato et al., 2011; Shenje et al., 2014) it is expected that mitochondrial activity will also be altered, as both processes are dependent on each other and regulated by cytoskeletal dynamics (Horbay and Bilyy, 2016).

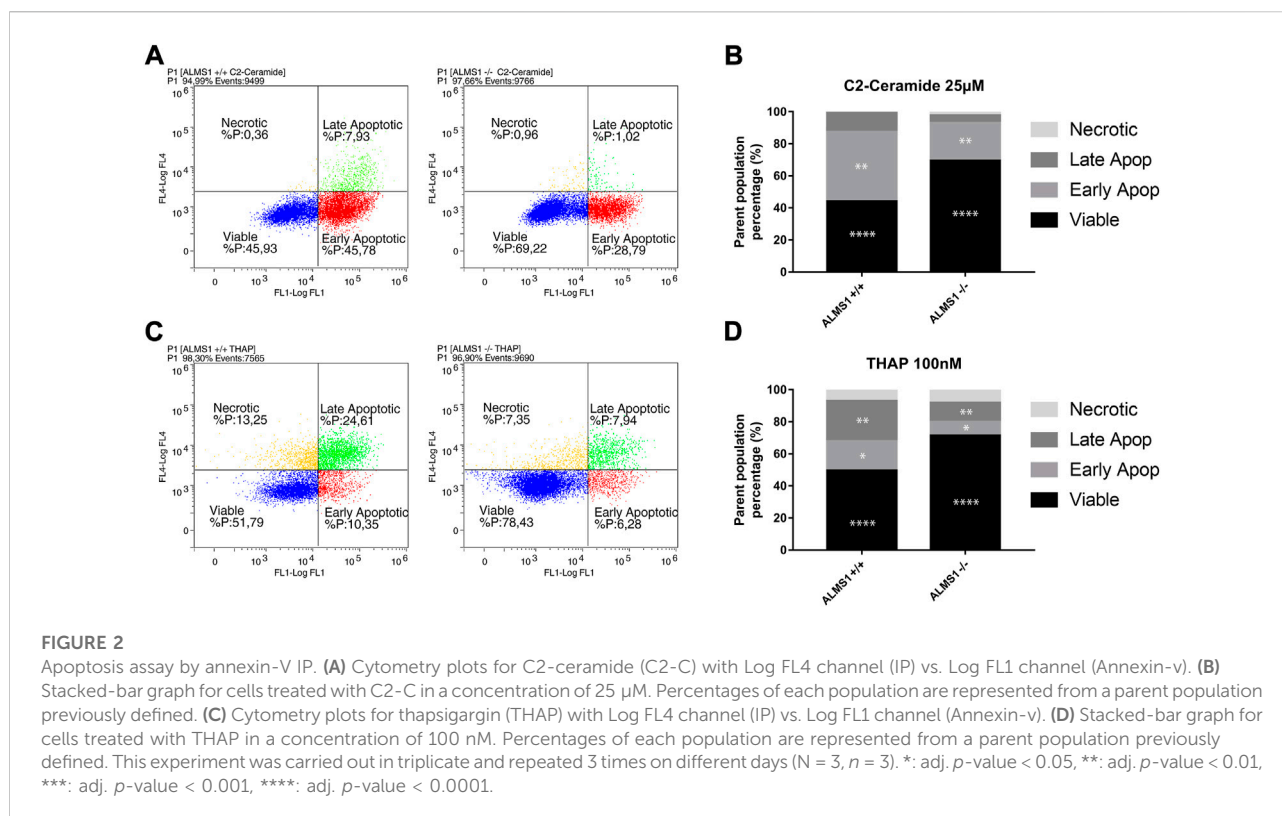
We evaluated the different phases of the cell cycle using the fox synchronous algorithm (Fox, 1980) to determine the Gaussian distribution of the different populations. DAPI fluorescence (461 nm) and events count (cells) were displayed in the plots (Figure 1A). After 24 h of incubation, HeLa cells *ALMS1* *-/-* shown a significantly reduction (*p*-value < 0.05) in S phase from 24.26% ± 1.32 in *ALMS1* *+/+* to 19.27% ± 1.69 in *ALMS1* *-/-*. The cell cycle arrest was caused by a significant

increase in the G2/M population (*p*-value < 0.01), from 1.6% ± 0.62 in *ALMS1* *+/+* to 4.88% ± 0.80 (Figure 1B). The results in the G0/G1 population did not show significant differences between genotypes. Despite this, the basal mitochondrial activity did not show a significant difference between *ALMS1* *+/+* and *ALMS1* *-/-* (Figure 1C).

The lack of *ALMS1* in HeLa prevents apoptosis induced by C2-ceramides and thapsigargin

Accumulation of cells in G2/M phase triggers apoptosis by different pathways such as caspases (Arita et al., 1997; Westrate et al., 2014). We evaluated whether these cells were sensitive to apoptosis in response to an ER stress-inducing stimulus (Thapsigargin; THAP) (Yoshida et al., 2006), and a pro-apoptotic sphingolipid such as C2-ceramide.

As in the cell cycle assay, initial isolation of the cell population (P1) of interest was performed. Plots were represented with the FL4 (7-AAD) fluorescence in the y-axis



and FL1 (Annexin V) fluorescence in the x-axis, both on a logarithmic scale. Thresholds for different populations (viable, early apoptotic, late apoptotic, and necrotic) were defined by a previous compensation analysis using THAP-like positive control of cell death. Finally, experiments were performed by triplicates in the plate ($n = 3$) and in 3 alternative days ($N = 3$).

Genotypes *ALMS1* $+/+$ and *ALMS1* $-/-$ showed significant differences in viable (44.02% and 69.49%, respectively) and early apoptotic (43.47% and 23.44%) populations in cells stimulated with C2-C (Figures 2A,B). Moreover, cells stimulated with THAP also showed significant differences between genotypes in viable (49.56% and 71.33%), early apoptotic (18.25% and 8.56%) and late apoptotic (25.09% and 11.93%) populations (Figures 2C,D). These results indicate a resistance to apoptosis for these stimuli due to the lack of the *ALMS1*.

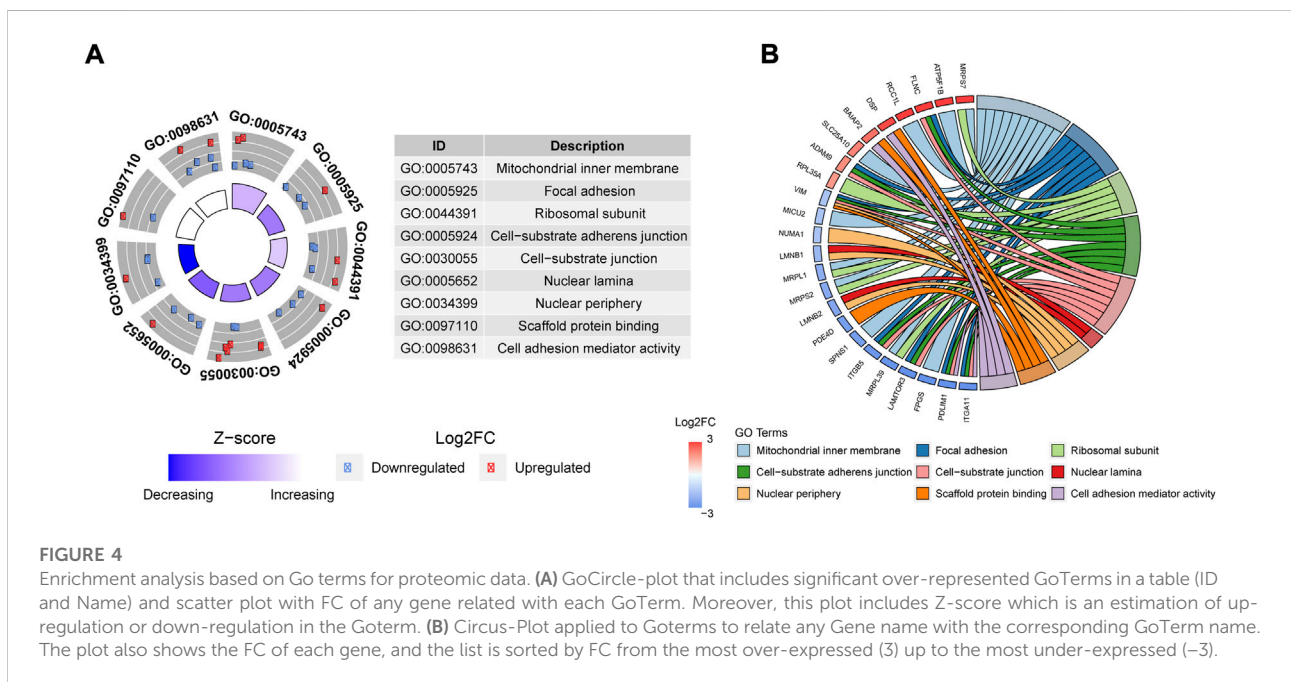
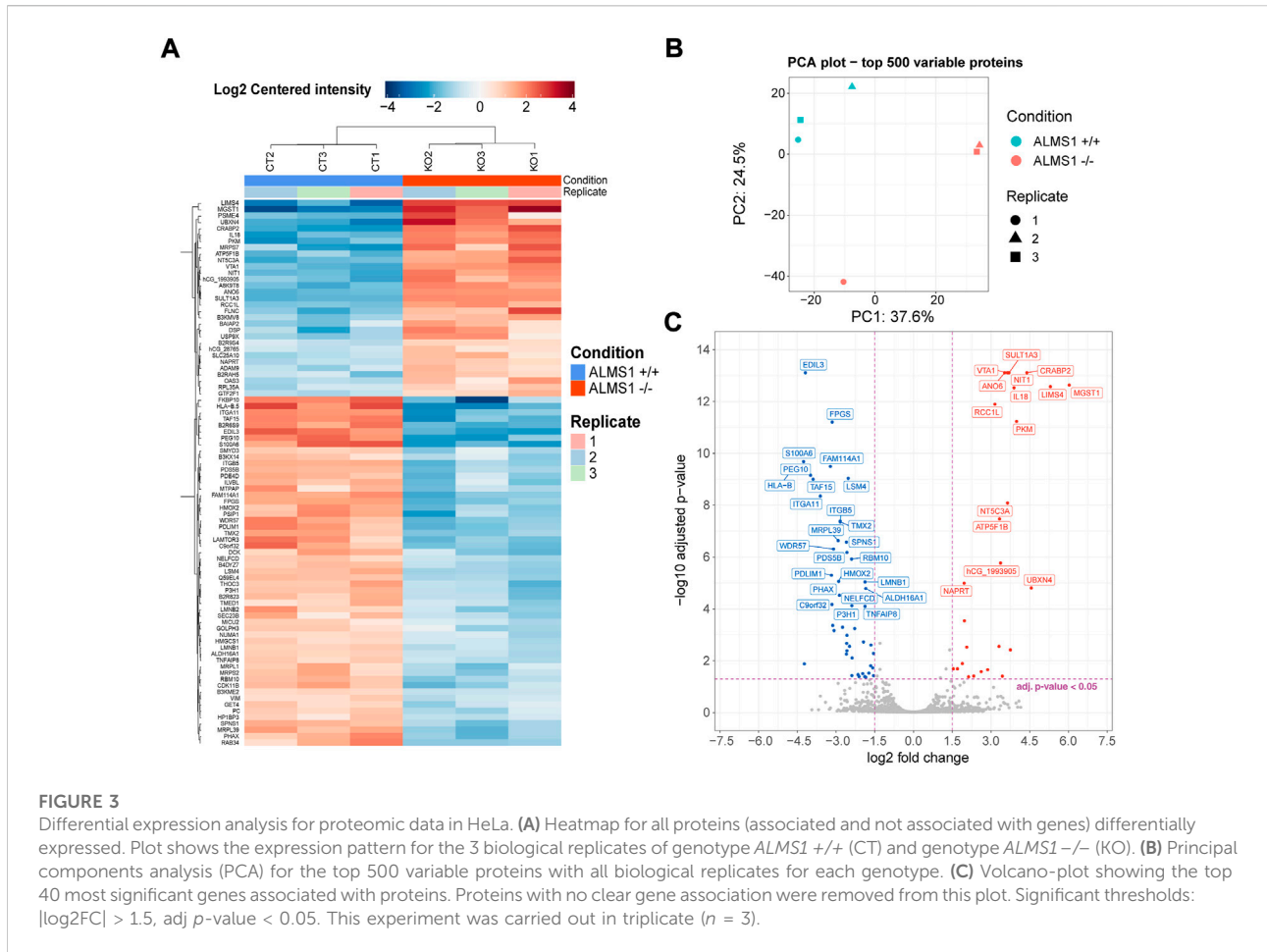
The proteomic profile in HeLa cells reveals *ALMS1* like a regulator of cell adhesion through the TGF- β pathway

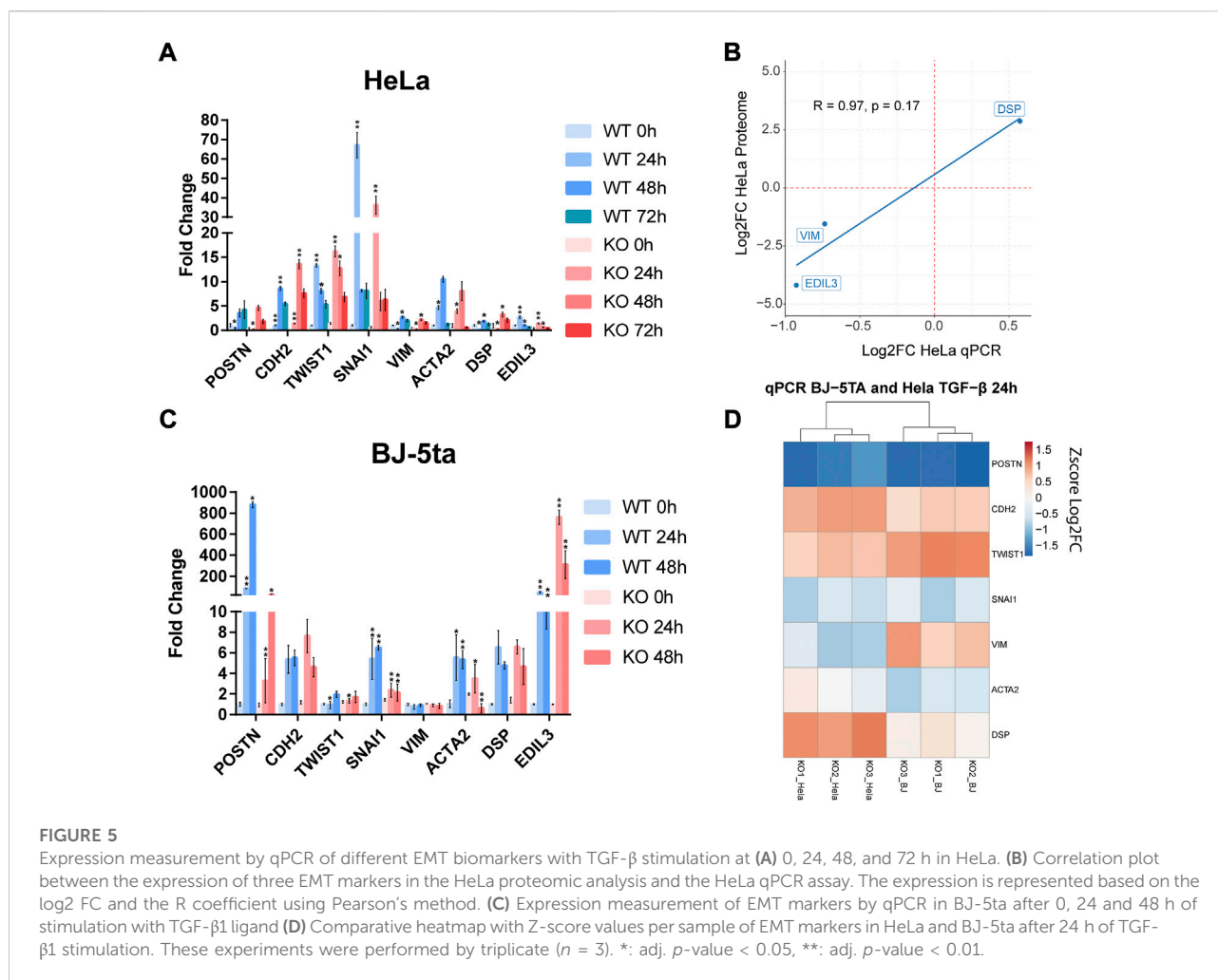
TGF- β is a pathway that plays a key role in the control of cell proliferation and apoptotic processes (Zhang et al., 2017). Since signal transduction through this pathway occurs *via* the primary cilium (Clement et al., 2013; Christensen et al., 2017), the lack of *ALMS1* could explain the aberrant processes seen above.

We evaluated how *ALMS1* depletion affects the signal transduction through stimulated TGF- β pathway. In this bulk analysis, we obtained a total of 86 differentially expressed proteins (DEP) (Figure 3A), 31 (36%) over-expressed and 55 (64%) under-expressed. The variation in protein expression in this dataset can be explained mainly by a single principal component (Figure 3B). This would make sense as the main difference between these two genotypes would be the presence or absence of the *ALMS1* gene. From this dataset, a total of 76 proteins were associated with genes (Figure 3C).

Based on the DE of protein-coding genes (PCG) we performed an enrichment analysis obtaining a total of 9 GO terms significantly overrepresented (adj. p -value < 0.05) (Figures 4A,B). The majority of these PCG were associated with focal adhesion, cell-cell or cell-substrate interactions. This result suggests the implication of *ALMS1* in the control of adhesion processes. In addition, we calculated the z-score of these GO terms (Figure 4A), showed a significant decrease in process related to the ability of these cells to properly migrate or adhere to each other or their matrix.

Moreover, genes such as vimentin (*VIM*) and desmoplakin (*DSP*), common biomarkers of EMT, were associated with these GO terms (Figure 4B). Interestingly, these genes exhibited an expression pattern opposite to that observed when EMT process is activated.





Finally, *ITGB5* and *ITGA11*, two integrins whose activation plays an important role in the normal development of EMT, proliferation and invasion are inhibited (Bianchi et al., 2010; Erusappan et al., 2019).

ALMS1 depletion alters the expression pattern of TGF- β 1-induced EMT markers in HeLa

Proteomic analysis showed alterations in several adhesion processes coupled with aberrant expression of EMT-related genes (*VIM*, *DSP*, *ITGB5*, and *ITGA11*). We measure the main EMT markers in our *ALMS1*-deficiency HeLa cells and compare it with another *ALMS1* model in the hTERT-BJ-5ta line.

We evaluated the expression of the principal EMT biomarkers (*SNAI1*, *CDH2*, *TWIST1*, *ACTA2*, *VIM*, and *DSP*) and other genes related to EMT (*POSTN*, *EDIL3*). We perform stimulations at different time points (24, 48 and 72 h for HeLa

and 24 and 48 h for BJ-5ta) with rh-TGF- β 1 (2 ng/ml) stimulation.

In HeLa (Figure 5A) at 24 h of stimulation *POSTN*, *SNAI1*, *VIM*, *ACTA2*, and *EDIL3* were found under-expressed, while *TWIST1* and *DSP* were over-expressed. This data confirms the expression pattern previously detected in the proteome analysis related to the genes *VIM*, *DSP* and *EDIL3* (Figure 5B). At 48 h of stimulation, the over-expressed genes *CDH2*, *TWIST1* and *DSP*, in addition to *EDIL3* and *VIM* inhibition, showed significant differences (Figure 5A). No other tested gene were significant. Finally, at 72 h of stimulation the expression pattern was like the previous stimulation time points. However, the data dispersion was too high, and no significant differences were detected.

In BJ-5ta (Figure 5C) no inhibition of *VIM* or overexpression of *DSP* were detected. However, inhibition of *POSTN* and the transcription factor (TF) *SNAI1* was persistent in both cell lines as well as the overexpression of *TWIST1*. *ACTA2* also showed decreased levels in HeLa but not as significant as in BJ-5ta. After Z score normalization of log₂FC both cell lines showed a similar expression pattern of these markers (Figure 5D). *EDIL3* is not

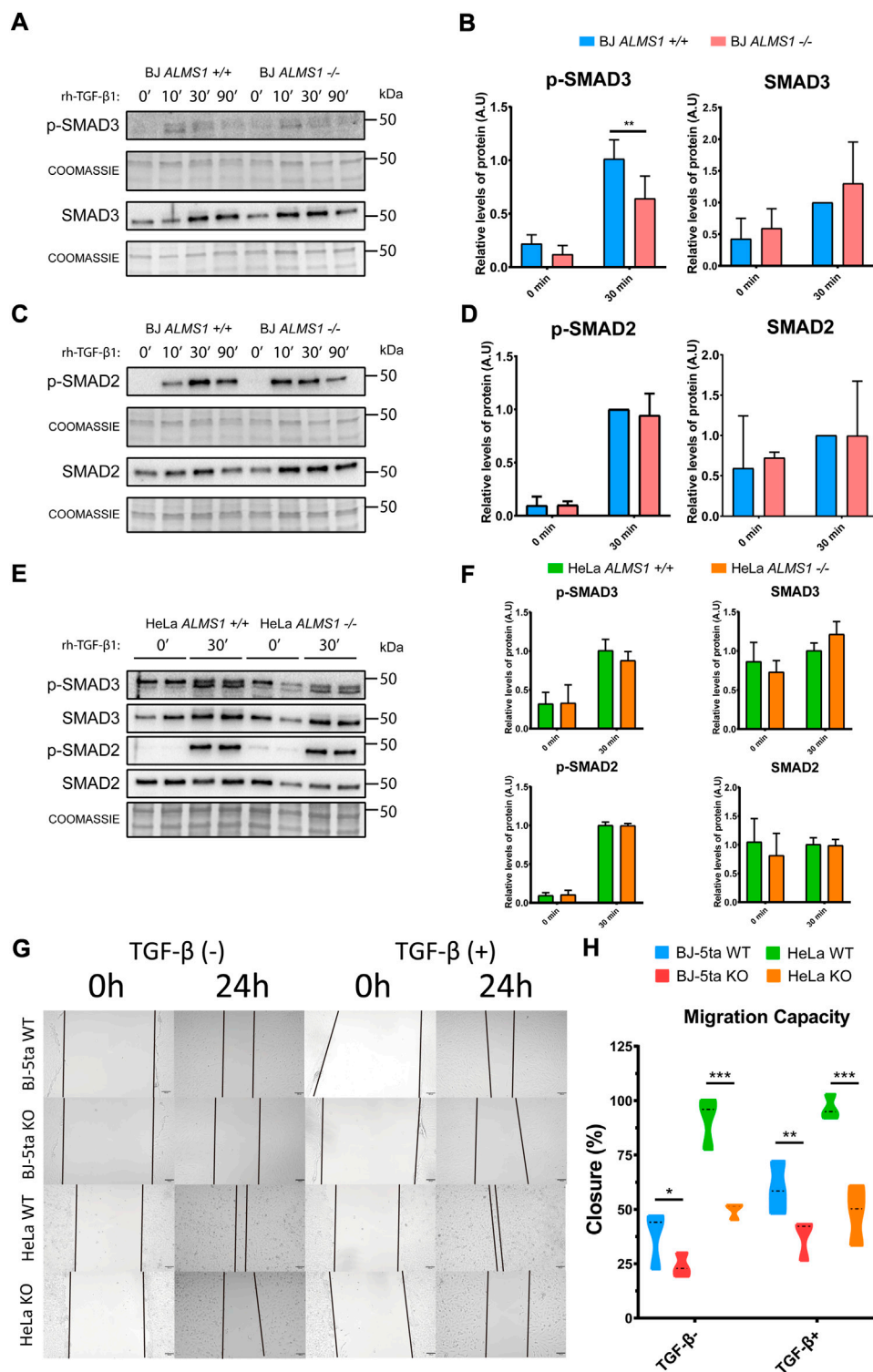


FIGURE 6

TGF-β canonical pathway activation assay and measurement of cell migration capacity in HeLa and BJ-5ta. (A) Representative western-blot of p-SMAD3 and SMAD3 levels after 0, 10, 30 and 90 min of stimulation with TGF-β1 (2 ng/μL) ligand and their corresponding loading controls (coomassie) in BJ-5ta cells (n = 3). (B) Quantification of band intensity in WB for p-SMAD3 and SMAD3 at time 0 and after 30 min stimulation with TGF-β1. *: p-value < 0.05, **: p-value < 0.01 (C) Representative western-blot of p-SMAD2 and SMAD2 levels after 0, 10, 30 and 90 min of stimulation with TGF-β1 (2 ng/μL) ligand and their corresponding loading controls (coomassie) in BJ-5ta cells (n = 3). (D) Quantification of band intensity in WB for p-SMAD2 and SMAD2 at time 0 and after 30 min stimulation with TGF-β1. *: p-value < 0.05, **: p-value < 0.01. (E) Representative (Continued)

FIGURE 6 (Continued)

western-blot of p-SMAD3, SMAD3, p-SMAD2 and SMAD2 levels after 0 and 30 min of stimulation with TGF- β 1 (2 ng/ μ L) ligand and their corresponding loading control (coomassie) in HeLa cells ($n = 2$). **(F)** Quantification of band intensity in WB for p-SMAD3, SMAD3, p-SMAD2 and SMAD2 at time 0 and after 30 min stimulation with TGF- β 1. *: p -value < 0.05, **: p -value < 0.01 **(G)** Representative images of wound healing assay in HeLa (WT and KO) and BJ-5ta (WT and KO) at 0 and 24 h in absence or presence of 2 ng/ μ L TGF- β 1. **(H)** Quantification of the cell area of the image and how it decreased after 24 h of incubation ($n = 3$). *: p -value < 0.05, **: p -value < 0.01, ***: p -value < 0.001.

shown in the heatmap as FC is too high, so it could mask the differences of the rest of the markers.

Absence of *ALMS1* decreases migration capacity in HeLa and BJ-5ta and reduce SMAD3 phosphorylation in BJ-5ta

We evaluated the canonical activation of the TGF- β pathway. SMAD2 and SMAD3 phosphorylation levels were analysed at 4 different times (0, 10, 30, and 90 min) in BJ-5ta and 2 different times (0 and 30 min) in HeLa after TGF- β 1 stimuli. The data shown that the lack of *ALMS1* inhibits SMAD3 (Ser213) activation after 30 min of TGF- β 1 ligand exposure (p -value < 0.01) but not affects to SMAD2 phosphorylation in BJ-5ta (Figures 6A-D). In HeLa cells no alterations in canonical pathway signalling of TGF- β were detected (Figure 6E,F). The p-SMADs/SMADs ratios did not differ from the p-SMADs/total protein ratios, data not shown.

Finally, we measured cell migration capacity in both cell lines in the presence and absence of -rh-TGF- β 1 ligand. (Figure 6G,H). *ALMS1* depletion reduced migration capacity compared to the control line in both cell lines. This reduction is exacerbated after TGF- β stimulation in BJ-5ta while in HeLa the tendency is the same in the presence or absence of the stimulus.

Discussion

In this study, our results were consistent with previously described cell cycle arrest (Shenje et al., 2014) and resistance to apoptosis (Zulato et al., 2011) in *ALMS1* deficiency cardiomyocytes and fibroblasts respectively. Moreover, we reported new insights to understand the role of *ALMS1* in cell function and TGF- β signalling.

Regarding mitochondrial activity, its reduction capacity does not seem to be affected by *ALMS1* depletion (Figure 1C). However, because certain proteins related to the mitochondrial inner membrane appear differentially expressed at the proteomic level (Figures 4A,B). Our data are not enough to rule out other alterations in mitochondrial biogenesis and functionality.

Cell cycle arrest in the G2/M phase (Figures 1A,B), also described in *ALMS1*-knockdown cardiomyocytes (Shenje et al., 2014), seems to be a cell process triggered by *ALMS1* depletion.

Several studies have already linked cell cycle arrest in the G2/M phase to the TGF- β pathway and the development of fibrosis (Yang et al., 2010; Li et al., 2016; White et al., 2021). Cell cycle arrest in G2/M is often accompanied by a decrease in cell proliferation. This is consistent with what has been described in patient fibroblasts (Zulato et al., 2011), but not in cardiomyocytes (Shenje et al., 2014). *ALMS1*-deficient cardiomyocytes show an increase in certain proliferative markers (PH3, Ki67 and EdU) despite having a cell cycle arrested in G2/M phase (Shenje et al., 2014). However, overexpression of these markers is not enough evidence that cytokinesis and karyokinesis are occurring correctly, and further investigation is required to determine whether *ALMS1*-deficient cells are hyperproliferative despite G2/M arrest and cell cycle elongation. In the case of Alström syndrome, dilated cardiomyopathy is a phenotype present in approximately two-thirds of patients, so it would be expected that *ALMS1* depletion was not enough for the appearance of this symptom (Marshall et al., 2011). Normally, cell cycle arrest in both the G2/M and G0/G1 phases is often accompanied by the activation of apoptotic processes (Jakubikova et al., 2005; Horbay and Bilyy, 2016; Madungwe et al., 2018; Liu et al., 2021). In contrast, depletion of *ALMS1* seems to generate apoptosis resistance against THAP and C2-C in HeLa cells (Figure 2), which is in accordance with that reported by Zulato et al. (2011) in patient fibroblasts. This imbalance between mitosis and apoptosis could be implicated in the development of fibrosis in patients with Alström syndrome.

THAP is a non-competitive inhibitor for Ca²⁺-ATPases located in the endoplasmic reticulum (SERCA). This, inhibits Ca²⁺ reflux to the lumen of the endoplasmic reticulum, generating endoplasmic reticulum stress (ER stress) (Lindner et al., 2020). At the same time, ER stress activates a signalling network called Unfolded Protein Response (UPR) which alleviates this stress and promotes cell survival, restoring ER homeostasis (Osowski and Urano, 2011). At this point, *ALMS1* depletion could be acting at two levels: inhibiting THAP action (ER stress) or over-activating UPR and generating apoptosis resistance. Because of the role of *ALMS1* in the centrosome and its relation with endocytic trafficking (Collin et al., 2012), its depletion could probably alter the structure of the membrane, inhibiting the signalling transduction of ligands like THAP. THAP also induces apoptosis impairing cytoskeleton dynamics and disorganization of F-actin via mTORC1 inhibition in the mTORC1-RhoA-Limk-Cofilin-1 axis in A549 cells (Wang et al., 2014). *ALMS1* depletion

already causes disorganization of the F-actin cytoskeleton (Collin et al., 2012) but does not lead to cell death. Probably, the mTOR pathway through mTORC1 was inhibited in *ALMS1* $-/-$ cells, but in this case, other mechanisms could prevent cells from reaching apoptotic stages. This would be supported by the inhibition of LAMTOR3 (Figure 4B), a protein involved in the formation of the Ragulator complex that activates mTORC1 (Mu et al., 2017).

C2-C is a sphingolipid that induces caspases-dependent apoptosis, inhibiting PI3K/AKT pathway and increasing the depolarisation of the mitochondrial membrane (Arora et al., 1997; Zinda et al., 2001; Sánchez-Mora et al., 2012). The over-activation of the PI3K/AKT pathway could explain the apoptotic resistance in the case of the C2-C (Fahy et al., 2003; Jeong et al., 2008). This fact would agree with the previous proposed mTORC1 inhibition, since phosphorylation of AKT/PKB at s473 leads to inhibition of mTORC1 mediated by FoxO transcription factors (Chen et al., 2010), which could be related to F-actin filament disorganisation previously described in Alström fibroblasts (Collin et al., 2012).

In addition to the role of *ALMS1* in G2/M phase cell cycle arrest and resistance to THAP- and C2-C-mediated apoptosis, this study suggests that *ALMS1* depletion leads to inhibition of TGF- β signalling pathway. This could be affecting downstream processes such as cell migration and adhesion.

After TGF- β stimulation, the lack of *ALMS1* alters the expression of several genes related to focal adhesion and cell-substrate adherens junction (Figures 4A,B), two processes required for TGF- β 1-induced EMT (Cicchini et al., 2008; Baronsky et al., 2017). This fact could be conditioning the activation of EMT, preventing cells from moving into a mesenchymal state characterised by an increased migratory capacity. Previous studies have demonstrated the relationship between signalling through the primary cilium and the EMT focusing mainly on signalling through the WNT and SHH pathway in various organs such as epicardial tissue, kidney epithelial cells, and pancreatic cells (Bailey et al., 2009; Saito et al., 2015; Blom and Feng, 2018; Han et al., 2018). However, signalling through the TGF- β pathway has not yet been extensively studied in this context.

Moreover, we have found interesting candidates in the HeLa proteome profiling that could explain or be related to the mentioned cellular disturbances (Figure 3C). *SI00A6*, under-expressed, is a positive regulator of proliferation, migration and angiogenesis (Li et al., 2017; Li et al., 2018; Li et al., 2019), and also a regulator of endothelial calcium signalling (Haldar et al., 2020). *PKM*, which was over-expressed in HeLa cells, is associated with apoptosis resistance (Calabretta et al., 2016). *ITGA11*, another gene under-expressed in this cell line and related to fibrosis generation, is expressed due to activation of the TGF- β pathway (Lu et al., 2010). Finally, two known EMT markers, *VIM* and *DSP*, showed a reverse pattern to that expected when this process is activated. *VIM* is a key player in the regulation of EMT and its deficiency leads to inhibition of this process

(Cheng et al., 2016). On the other hand, *DSP* is a protein involved in cell-cell junctions mediated by desmosomes. It is therefore considered a typical epithelial marker whose decrease is related to the passage of the cell from an epithelial to a mesenchymal state (Serrano-Gomez et al., 2016). This could be first evidence suggesting inhibition of the TGF- β 1-induced EMT when *ALMS1* is missing.

One of the most relevant detected genes was *SNAI1*, which is inhibited in both cell lines (HeLa and BJ-5ta). *SNAI1* and *TWIST1* are transcription factors that repress E-cadherin (*CDH1*) expression and activate the expression of N-cadherins (*CDH2*) (Poser et al., 2001; Jiao et al., 2002). E/N-cadherins switch is involved in the induction of EMT (Gravdal et al., 2007; Hao et al., 2012) through the TGF- β pathway (Araki et al., 2011). Inhibition of *SNAI1* could be affecting the normal EMT in these cells. The decreased expression of *SNAI1*, together with the inhibition of *ACTA2* and *POSTN*, also suggests that TGF- β 1-induced EMT would be down-regulated. *SNAI1* is up-regulated by SMAD3, which is phosphorylated when the TGF- β pathway is activated and forms a complex with SMAD2 (Nakao et al., 1997). The phosphorylated SMAD2-SMAD3 complex translocate to the nucleus, activating the expression of several genes related to cell migration and EMT such as *SNAI1* (Roberts et al., 2006). Because we detected consistent inhibition in both cell models of *SNAI1*, we sought to determine whether SMAD3 and SMAD2 activation was also compromised in BJ-5ta and HeLa models. In BJ-5ta, we conclude that *ALMS1* depletion inhibits SMAD3 phosphorylation but not affect SMAD2 phosphorylation (Figures 6A–D). This fact could lead to downstream inhibition of *SNAI1* and affect migration and adhesion capacity in this cell line (Figure 6G,H). In HeLa, no alterations in the activation of the canonical TGF- β pathway were detected (Figure 6E,F). In addition, a decrease in cell migration capacity was observed, but independently of TGF- β , in contrast to BJ-5ta (Figure 6G,H). This could explain that the involvement of *ALMS1* in cell migration is a conserved process, but its regulation is a cell type-dependent process.

We have previously described that *ALMS1* depletion by siRNA inhibits SMAD2 phosphorylation in the hTERT RPE-1 cell line (Álvarez-Satta et al., 2021) but this was not detected in any of our KO models. The only alteration detected in the canonical pathway was the inhibition of SMAD3 activation in BJ-5ta. This difference could be due to the cell type or to differences between the KO and siRNA models. Because the results were consistent in both KO models, the discrepancies with the siRNA model appear to be technique-dependent, which have been described with other genes such as *DOCK6* (Cerikan et al., 2016). In addition, CRISPR assays appear to have a higher specificity than siRNA assays, which would lend greater veracity to the results presented in this study (Smith et al., 2017).

This facts leads us to hypothesise that inhibition of p-SMAD3 could prevent the formation of the SMAD2/3 complex, affecting the expression of *SNAI1* in BJ-5ta (Vincent et al., 2009). Whereas in HeLa, inhibition of *SNAI1* and cell migration capacity appears to involve other regulatory mechanisms. Alström syndrome is a

rare disease with a very heterogeneous phenotype. Difficult access to patient samples and the limited literature on this disease greatly complicate its study. To date, the role of the *ALMS1* gene has not been linked to specific cellular processes with enough strength to determine a pathological mechanism to explain the multiple manifestations of the disease. The phenotypic heterogeneity of the main symptoms could be explained by a context-specific role of the *ALMS1* gene. Before we can provide a mechanistic model of the disease, we must determine the common and the tissue-specific functions of the *ALMS1* gene. This study reinforces the role of the *ALMS1* gene in cell cycle regulation and apoptosis and suggests new functions such as the regulation of EMT or cell adhesion processes, opening new avenues for future research. Finally, phenotypic heterogeneity in less common symptoms such as dilated cardiomyopathy could be due to the mutational load of each patient that could be affecting different modulatory genes.

The main limitations of this study are due to the use of immortalised cell models. Although they are widely used in research, validation in patients cells or animal models is necessary. Therefore, we have taken into account the common results in both models, focusing on processes rather than specific genes.

Conclusion

ALMS1 have a role in the regulation of cell cycle and apoptotic processes but does not affect mitochondrial reduction capacity in HeLa. *ALMS1* depletion affects signal transduction through the TGF- β pathway, altering the expression of several EMT-related genes in BJ-5ta and HeLa. However, the canonical (SMAD-dependent) pathway did not show major differences. Finally downstream processes such as cell migration and adhesion capacity appear to be compromised in the absence of *ALMS1*.

Data availability statement

The datasets presented in this study can be found in online repositories. The names of the repository/repositories and accession number(s) can be found below: The mass spectrometry proteomics data have been deposited to the ProteomeXchange Consortium *via* the PRIDE (Perez-Riverol et al., 2019) partner repository with the dataset identifier PXD024964.

Author contributions

BB-M and DV designed the study. BB-M performed the experiments and analysed the data. EN-G assisted in performing apoptosis, cell cycle and mitochondrial activity assays. AI-R

assisted in the quantification of the expression of EMT markers in the BJ-5ta model and in the cell migration assay. BB-M and DV wrote the manuscript. All authors have read the draft and provided approval for publication.

Funding

This work was funded by Instituto de Salud Carlos III (project PI15/00049 and PI19/00332), Xunta de Galicia (Centro de Investigación de Galicia CINBIO 2019-2022; Ref. ED431G-2019/06) and Consolidación e estruturación de unidades de investigación competitivas e outras accións de fomento (Xunta de Galicia, ED431C-2018/54). Brais Bea Mascato (FPU17/01567) was supported by graduate studentship awards (FPU predoctoral fellowship) from the Spanish Ministry of Education, Culture and Sports.

Acknowledgments

We sincerely thank the Proteomics and Genomics services from Centro de Apoyo Científico-Tecnológico a la Investigación (CACTI) of University of Vigo and its specialists Paula Álvarez Chaver, Ángel Sebastián Comesaña, Verónica Outeiriño and Manuel Marcos for their guidance and advise. We also thank Mercedes Peleteiro Olmedo from Centro de Investigacións Biomédicas (CINBIO) from University of Vigo for the flow cytometry service.

Conflict of interest

The authors declare that the research was conducted in the absence of any commercial or financial relationships that could be construed as a potential conflict of interest.

Publisher's note

All claims expressed in this article are solely those of the authors and do not necessarily represent those of their affiliated organizations, or those of the publisher, the editors and the reviewers. Any product that may be evaluated in this article, or claim that may be made by its manufacturer, is not guaranteed or endorsed by the publisher.

Supplementary material

The Supplementary Material for this article can be found online at: <https://www.frontiersin.org/articles/10.3389/fmolb.2022.992313/full#supplementary-material>

References

- Álvarez-Satta, M., Lago-Docampo, M., Bea-Mascato, B., Solarat, C., Castro-Sánchez, S., Christensen, S. T., et al. (2021). ALMS1 regulates TGF- β signaling and morphology of primary cilia. *Front. Cell Dev. Biol.* 9, 623829. doi:10.3389/fcell.2021.623829
- Araki, K., Shimura, T., Suzuki, H., Tsutsumi, S., Wada, W., Yajima, T., et al. (2011). E/N-cadherin switch mediates cancer progression via TGF- β -induced epithelial-to-mesenchymal transition in extrahepatic cholangiocarcinoma. *Br. J. Cancer* 105, 1885–1893. doi:10.1038/bjc.2011.452
- Arita, D., Kambe, M., Ishioka, C., and Kanamaru, R. (1997). Induction of p53-independent apoptosis associated with G2M arrest following DNA damage in human colon cancer cell lines. *Jpn. J. Cancer Res.* 88, 39–43. doi:10.1111/j.1349-7006.1997.tb00299.x
- Arora, A. S., Jones, B. J., Patel, T. C., Bronk, S. F., and Gores, G. J. (1997). Ceramide induces hepatocyte cell death through disruption of mitochondrial function in the rat. *Hepatology* 25, 958–963. doi:10.1002/hep.510250428
- Bailey, J. M., Mohr, A. M., and Hollingsworth, M. A. (2009). Sonic hedgehog paracrine signaling regulates metastasis and lymphangiogenesis in pancreatic cancer. *Oncogene* 28, 3513–3525. doi:10.1038/onc.2009.220
- Baronsky, T., Ruhlandt, D., Brückner, B. R., Schäfer, J., Karedla, N., Isbaner, S., et al. (2017). Cell-substrate dynamics of the epithelial-to-mesenchymal transition. *Nano Lett.* 17, 3320–3326. doi:10.1021/acs.nanolett.7b01558
- Bianchi, A., Gervasi, M. E., and Bakin, A. (2010). Role of β 5-integrin in epithelial-mesenchymal transition in response to TGF- β . *Cell Cycle* 9, 1647–1659. doi:10.4161/cc.9.8.11517
- Blom, J. N., and Feng, Q. (2018). Cardiac repair by epicardial EMT: Current targets and a potential role for the primary cilium. *Pharmacol. Ther.* 186, 114–129. doi:10.1016/j.pharmthera.2018.01.002
- Calabretta, S., Bielli, P., Passacantilli, I., Pilozi, E., Fendrich, V., Capurso, G., et al. (2016). Modulation of PKM alternative splicing by PTBP1 promotes gemcitabine resistance in pancreatic cancer cells. *Oncogene* 35, 2031–2039. doi:10.1038/onc.2015.270
- Cerikan, B., Shaheen, R., Colo, G. P., Gläfer, C., Hata, S., Knobloch, K.-P., et al. (2016). Cell-intrinsic adaptation arising from chronic ablation of a key Rho GTPase regulator. *Dev. Cell* 39, 28–43. doi:10.1016/j.devcel.2016.08.020
- Chen, C.-C., Jeon, S.-M., Bhaskar, P. T., Nogueira, V., Sundararajan, D., Tonic, I., et al. (2010). FoxOs inhibit mTORC1 and activate akt by inducing the expression of Sestrin3 and rictor. *Dev. Cell* 18, 592–604. doi:10.1016/j.devcel.2010.03.008
- Cheng, F., Shen, Y., Mohanasundaram, P., Lindström, M., Ivaska, J., Ny, T., et al. (2016). Vimentin coordinates fibroblast proliferation and keratinocyte differentiation in wound healing via TGF- β -Slug signaling. *Proc. Natl. Acad. Sci. U. S. A.* 113, E4320–E4327. doi:10.1073/pnas.1519197113
- Christensen, S. T., Morthorst, S. K., Mogensen, J. B., and Pedersen, L. B. (2017). Primary cilia and coordination of receptor tyrosine kinase (RTK) and transforming growth factor β (TGF- β) signaling. *Cold Spring Harb. Perspect. Biol.* 9, a028167. doi:10.1101/cshperspect.a028167
- Cicchini, C., Laudadio, I., Citarella, F., Corazzari, M., Steindler, C., Conigliaro, A., et al. (2008). TGF β -induced EMT requires focal adhesion kinase (FAK) signaling. *Exp. Cell Res.* 314, 143–152. doi:10.1016/j.yexcr.2007.09.005
- Clement, C. A., Ajbro, K. D., Koefoed, K., Vestergaard, M. L., Veland, I. R., Henriques de Jesus, M. P. R., et al. (2013). TGF- β signaling is associated with endocytosis at the pocket region of the primary cilium. *Cell Rep.* 3, 1806–1814. doi:10.1016/j.celrep.2013.05.020
- Collin, G. B., Marshall, J. D., Ikeda, A., So, W. V., Russell-Eggitt, I., Maffei, P., et al. (2002). Mutations in ALMS1 cause obesity, type 2 diabetes and neurosensory degeneration in Alström syndrome. *Nat. Genet.* 31, 74–78. doi:10.1038/ng867
- Collin, G. B., Marshall, J. D., King, B. L., Milan, G., Maffei, P., Jagger, D. J., et al. (2012). The Alström syndrome protein, ALMS1, interacts with α -actinin and components of the endosome recycling pathway. *PLoS One* 7, e37925. doi:10.1371/journal.pone.0037925
- Erusappan, P., Alam, J., Lu, N., Zeltz, C., and Gullberg, D. (2019). Integrin α 11 cytoplasmic tail is required for FAK activation to initiate 3D cell invasion and ERK-mediated cell proliferation. *Sci. Rep.* 9, 15283. doi:10.1038/s41598-019-51689-6
- Fahy, B. N., Schlieman, M., Virudachalam, S., and Bold, R. J. (2003). AKT inhibition is associated with chemosensitisation in the pancreatic cancer cell line MIA-PaCa-2. *Br. J. Cancer* 89, 391–397. doi:10.1038/sj.bjc.6601037
- Fox, M. H. (1980). A model for the computer analysis of synchronous DNA distributions obtained by flow cytometry. *Cytometry* 1, 71–77. doi:10.1002/cyto.990010114
- Gravdal, K., Halvorsen, O. J., Haukaas, S. A., and Akslen, L. A. (2007). A switch from E-cadherin to N-cadherin expression indicates epithelial to mesenchymal transition and is of strong and independent importance for the progress of prostate cancer. *Clin. Cancer Res.* 13, 7003–7011. doi:10.1158/1078-0432.CCR-07-1263
- Gürtler, A., Kunz, N., Gomolka, M., Hornhardt, S., Friedl, A. A., McDonald, K., et al. (2013). Stain-Free technology as a normalization tool in Western blot analysis. *Anal. Biochem.* 433, 105–111. doi:10.1016/j.ab.2012.10.010
- Haldar, B., Hamilton, C. L., Solodushko, V., Abney, K. A., Alexeyev, M., Honkanen, R. E., et al. (2020). S100A6 is a positive regulator of PPP5C-FKBP51-dependent regulation of endothelial calcium signaling. *FASEB J. Off. Publ. Fed. Am. Soc. Exp. Biol.* 34, 3179–3196. doi:10.1096/fj.201901777R
- Han, S. J., Jung, J. K., Im, S. S., Lee, S. R., Jang, B. C., Park, K. M., et al. (2018). Deficiency of primary cilia in kidney epithelial cells induces epithelial to mesenchymal transition. *Biochem. Biophys. Res. Commun.* 496, 450–454. doi:10.1016/j.bbrc.2018.01.079
- Hao, L., Ha, J. R., Kuzel, P., Garcia, E., and Persad, S. (2012). Cadherin switch from E- to N-cadherin in melanoma progression is regulated by the PI3K/PTEN pathway through Twist and Snail. *Br. J. Dermatol.* 166, 1184–1197. doi:10.1111/j.1365-2133.2012.10824.x
- Hearn, T., Spalluto, C., Phillips, V. J., Renforth, G. L., Copin, N., Hanley, N. A., et al. (2005). Subcellular localization of ALMS1 supports involvement of centrosome and basal body dysfunction in the pathogenesis of obesity, insulin resistance, and type 2 diabetes. *Diabetes* 54, 1581–1587. doi:10.2337/diabetes.54.5.1581
- Horbay, R., and Bilyy, R. (2016). Mitochondrial dynamics during cell cycling. *Apoptosis* 21, 1327–1335. doi:10.1007/s10495-016-1295-5
- Jagger, D., Collin, G., Kelly, J., Towers, E., Nevill, G., Longo-Guess, C., et al. (2011). Alström Syndrome protein ALMS1 localizes to basal bodies of cochlear hair cells and regulates cilium-dependent planar cell polarity. *Hum. Mol. Genet.* 20, 466–481. doi:10.1093/hmg/ddq493
- Jakubikova, J., Bao, Y., and Sedlak, J. (2005). Isothiocyanates induce cell cycle arrest, apoptosis and mitochondrial potential depolarization in HL-60 and multidrug-resistant cell lines. *Anticancer Res.* 25, 3375–3386. Available at: <https://pubmed.ncbi.nlm.nih.gov/16101152/> (Accessed August 17, 2022).
- Jaykumar, A. B., Caceres, P., Henson, E. L., Beierwaltes, W. H., and Ortiz, P. A. (2017). Deletion of ALMS1 (Alström Syndrome 1) enhances salt-sensitive hypertension, and induces insulin resistance and obesity in rats. *FASEB J.* 31, 857.26. doi:10.1096/fasebj.31.1_supplement.857.26
- Jeong, S.-J., Dasgupta, A., Jung, K.-J., Um, J.-H., Burke, A., Park, H. U., et al. (2008). PI3K/AKT inhibition induces caspase-dependent apoptosis in HTLV-1-transformed cells. *Virology* 370, 264–272. doi:10.1016/j.virol.2007.09.003
- Jiao, W., Miyazaki, K., and Kitajima, Y. (2002). Inverse correlation between E-cadherin and Snail expression in hepatocellular carcinoma cell lines *in vitro* and *in vivo*. *Br. J. Cancer* 86, 98–101. doi:10.1038/sj.bjc.6600017
- Leitch, C. C., Lodh, S., Prieto-Echagüe, V., Badano, J. L., and Zaghoul, N. A. (2014). Basal body proteins regulate Notch signaling through endosomal trafficking. *J. Cell Sci.* 127, 2407–2419. doi:10.1242/jcs.130344
- Li, A., Gu, Y., Li, X., Sun, H., Zha, H., Xie, J., et al. (2018). S100A6 promotes the proliferation and migration of cervical cancer cells via the PI3K/Akt signaling pathway. *Oncol. Lett.* 15, 5685–5693. doi:10.3892/ol.2018.8018
- Li, A., Shi, D., Xu, B., Wang, J., Tang, Y.-L., Xiao, W., et al. (2017). S100A6 promotes cell proliferation in human nasopharyngeal carcinoma via the p38/MAPK signaling pathway. *Mol. Carcinog.* 56, 972–984. doi:10.1002/mc.22563
- Li, G., Vega, R., Nelms, K., Gekakis, N., Goodnow, C., McNamara, P., et al. (2007). A role for Alström syndrome protein, alms1, in kidney ciliogenesis and cellular quiescence. *PLoS Genet.* 3, e8. doi:10.1371/journal.pgen.0030008
- Li, H., Peng, X., Wang, Y., Cao, S., Xiong, L., Fan, J., et al. (2016). Atg5-mediated autophagy deficiency in proximal tubules promotes cell cycle G2/M arrest and renal fibrosis. *Autophagy* 12, 1472–1486. doi:10.1080/15548627.2016.1190071
- Li, P., Lv, X., Zhang, Z., and Xie, S. (2019). S100A6/miR193a regulates the proliferation, invasion, migration and angiogenesis of lung cancer cells through the P53 acetylation. *Am. J. Transl. Res.* 11, 4634–4649.
- Lindner, P., Christensen, S. B., Nissen, P., Möller, J. V., and Engedal, N. (2020). Cell death induced by the ER stressor thapsigargin involves death receptor 5, a non-autophagic function of MAP1LC3B, and distinct contributions from unfolded protein response components. *Cell Commun. Signal.* 18, 12. doi:10.1186/s12964-019-0499-z
- Liu, Y., Piao, X. J., Xu, W. T., Zhang, Y., Zhang, T., Xue, H., et al. (2021). Calycosin induces mitochondrial-dependent apoptosis and cell cycle arrest, and inhibits cell

- migration through a ROS-mediated signaling pathway in HepG2 hepatocellular carcinoma cells. *Toxicol. Vitro* 70, 105052. doi:10.1016/j.tiv.2020.105052
- Lu, N., Carracedo, S., Ranta, J., Heuchel, R., Soininen, R., and Gullberg, D. (2010). The human alpha11 integrin promoter drives fibroblast-restricted expression *in vivo* and is regulated by TGF-beta1 in a Smad- and Sp1-dependent manner. *Matrix Biol.* 29, 166–176. doi:10.1016/j.matbio.2009.11.003
- Luo, K. (2017). Signaling cross talk between TGF-beta/smad and other signaling pathways. *Cold Spring Harb. Perspect. Biol.* 9, a022137. doi:10.1101/CSHPERSPECT.A022137
- Madungwe, N. B., Feng, Y., Lie, M., Tombo, N., Liu, L., Kaya, F., et al. (2018). Mitochondrial inner membrane protein (Mitofilin) knockdown induces cell death by apoptosis via an AIF-PARP-dependent mechanism and cell cycle arrest. *Am. J. Physiol. Cell Physiol.* 315, C28–C43. doi:10.1152/ajpcell.00230.2017
- Marshall, J. D., Hinman, E. G., Collin, G. B., Beck, S., Cerqueira, R., Maffei, P., et al. (2007). Spectrum of ALMS1 variants and evaluation of genotype-phenotype correlations in Alström syndrome. *Hum. Mutat.* 28, 1114–1123. doi:10.1002/humu.20577
- Marshall, J. D., Maffei, P., Collin, G. B., and Naggert, J. K. (2011). Alström syndrome: Genetics and clinical overview. *Curr. Genomics* 12, 225–235. doi:10.2174/138920211795677912
- Massagué, J. (2012). TGF-beta signalling in context. *Nat. Rev. Mol. Cell Biol.* 13, 616–630. doi:10.1038/nrm3434
- Mönnich, M., Borgeskov, L., Breslin, L., Jakobsen, L., Rogowski, M., Doganli, C., et al. (2018). CEP128 localizes to the subdistal appendages of the mother centriole and regulates TGF-beta/BMP signaling at the primary cilium. *Cell Rep.* 22, 2584–2592. doi:10.1016/j.celrep.2018.02.043
- Mu, Z., Wang, L., Deng, W., Wang, J., and Wu, G. (2017). Structural insight into the Regulator complex which anchors mTORC1 to the lysosomal membrane. *Cell Discov.* 3, 17049. doi:10.1038/celldisc.2017.49
- Nakao, A., Imamura, T., Souchelnytskyi, S., Kawabata, M., Ishisaki, A., Oeda, E., et al. (1997). TGF-B receptor-mediated signalling through Smad2, Smad3 and Smad4. *EMBO J.* 16, 5353–5362. doi:10.1093/EMBOJ/16.17.5353
- Oslowski, C. M., and Urano, F. (2011). Measuring ER stress and the unfolded protein response using mammalian tissue culture system. *Methods Enzymol.* 490, 71–92. doi:10.1016/B978-0-12-385114-7.00004-0
- Perez-Riverol, Y., Csordas, A., Bai, J., Bernal-Llinares, M., Hewapathirana, S., Kundu, D. J., et al. (2019). The PRIDE database and related tools and resources in 2019: Improving support for quantification data. *Nucleic Acids Res.* 47, D442–D450. doi:10.1093/nar/gky1106
- Poser, I., Domínguez, D., de Herreros, A. G., Varnai, A., Buettner, R., and Bosserhoff, A. K. (2001). Loss of E-cadherin expression in melanoma cells involves up-regulation of the transcriptional repressor snail. *J. Biol. Chem.* 276, 24661–24666. doi:10.1074/jbc.M011224200
- Roberts, A. B., Tian, F., Byfield, S. D. C., Stuelten, C., Ooshima, A., Saika, S., et al. (2006). Smad3 is key to TGF-beta-mediated epithelial-to-mesenchymal transition, fibrosis, tumor suppression and metastasis. *Cytokine Growth Factor Rev.* 17, 19–27. doi:10.1016/j.cytogfr.2005.09.008
- Saito, S., Tampe, B., Müller, G. A., and Zeisberg, M. (2015). Primary cilia modulate balance of canonical and non-canonical Wnt signaling responses in the injured kidney. *Fibrogenes. Tissue Repair* 8, 6–11. doi:10.1186/s13069-015-0024-y
- Sánchez-Mora, R. M., Arboleda, H., and Arboleda, G. (2012). PINK1 overexpression protects against C2-ceramide-Induced CAD cell death through the PI3K/AKT pathway. *J. Mol. Neurosci.* 47, 582–594. doi:10.1007/s12031-011-9687-z
- Sanjana, N. E., Shalem, O., and Zhang, F. (2014). Improved vectors and genome-wide libraries for CRISPR screening. *Nat. Methods* 11, 783–784. doi:10.1038/nmeth.3047
- Schneider, C. A., Rasband, W. S., and Eliceiri, K. W. (2012). NIH image to ImageJ: 25 years of image analysis. *Nat. Methods* 9, 671–675. doi:10.1038/nmeth.2089
- Serrano-Gomez, S. J., Maziveyi, M., and Alahari, S. K. (2016). Regulation of epithelial-mesenchymal transition through epigenetic and post-translational modifications. *Mol. Cancer* 15, 18. doi:10.1186/s12943-016-0502-x
- Shenje, L. T., Andersen, P., Halushka, M. K., Lui, C., Fernandez, L., Collin, G. B., et al. (2014). Mutations in Alström protein impair terminal differentiation of cardiomyocytes. *Nat. Commun.* 5, 3416. doi:10.1038/ncomms4416
- Smith, I., Greenside, P. G., Natoli, T., Lahr, D. L., Wadden, D., Tirosh, I., et al. (2017). Evaluation of RNAi and CRISPR technologies by large-scale gene expression profiling in the Connectivity Map. *PLoS Biol.* 15, e2003213. doi:10.1371/journal.pbio.2003213
- Suarez-Arnedo, A., Figueroa, F. T., Clavijo, C., Arbeláez, P., Cruz, J. C., and Muñoz-Camargo, C. (2020). An image J plugin for the high throughput image analysis of *in vitro* scratch wound healing assays. *PLoS One* 15, e0232565. doi:10.1371/JOURNAL.PONE.0232565
- Thuault, S., Tan, E.-J., Peinado, H., Cano, A., Heldin, C.-H., and Moustakas, A. (2008). HMG2 and smads Co-regulate SNAIL1 expression during induction of epithelial-to-mesenchymal transition. *J. Biol. Chem.* 283, 33437–33446. doi:10.1074/JBC.M802016200
- Vincent, T., Neve, E. P. A., Johnson, J. R., Kukalev, A., Rojo, F., Albanell, J., et al. (2009). A SNAIL1-SMAD3/4 transcriptional repressor complex promotes TGF-beta mediated epithelial-mesenchymal transition. *Nat. Cell Biol.* 11, 943–950. doi:10.1038/ncb1905
- Walter, W., Sánchez-Cabo, F., and Ricote, M. (2015). GOpot: an R package for visually combining expression data with functional analysis. *Bioinformatics* 31, 2912–2914. doi:10.1093/bioinformatics/btv300
- Walton, K. L., Johnson, K. E., and Harrison, C. A. (2017). Targeting TGF-beta mediated SMAD signaling for the prevention of fibrosis. *Front. Pharmacol.* 8, 461. doi:10.3389/fphar.2017.00461
- Wang, F., Liu, D., Xu, H., Li, Y., Wang, W., Liu, B., et al. (2014). Thapsigargin induces apoptosis by impairing cytoskeleton dynamics in human lung adenocarcinoma cells. *ScientificWorldJournal.* 2014, 619050. doi:10.1155/2014/619050
- Wang, Y., Shi, J., Chai, K., Ying, X., and Zhou, B. P. (2013). The role of snail in EMT and tumorigenesis. *Curr. Cancer Drug Targets* 13 (9), 963–972. doi:10.2174/15680096113136660102
- Westrate, L. M., Sayfie, A. D., Burgenske, D. M., and MacKeigan, J. P. (2014). Persistent mitochondrial hyperfusion promotes G2/M accumulation and caspase-dependent cell death. *PLoS One* 9, 91911. doi:10.1371/journal.pone.0091911
- White, T. L., Deshpande, N., Kumar, V., Gauthier, A. G., and Jurkunas, U. V. (2021). Cell cycle re-entry and arrest in G2/M phase induces senescence and fibrosis in Fuchs Endothelial Corneal Dystrophy. *Free Radic. Biol. Med.* 164, 34–43. doi:10.1016/j.freeradbiomed.2020.12.445
- Yan, X., Liao, H., Cheng, M., Shi, X., Lin, X., Feng, X.-H., et al. (2016). Smad7 protein interacts with receptor-regulated smads (R-Smads) to inhibit transforming growth factor-beta (TGF-beta)/Smad signaling. *J. Biol. Chem.* 291, 382–392. doi:10.1074/JBC.M115.694281
- Yang, L., Besschetnova, T. Y., Brooks, C. R., Shah, J. V., and Bonventre, J. V. (2010). Epithelial cell cycle arrest in G2/M mediates kidney fibrosis after injury. *Nat. Med.* 16, 535–543. doi:10.1038/nm.2144
- Yoshida, I., Monji, A., Tashiro, K., Nakamura, K., Inoue, R., and Kanba, S. (2006). Depletion of intracellular Ca2+ store itself may be a major factor in thapsigargin-induced ER stress and apoptosis in PC12 cells. *Neurochem. Int.* 48, 696–702. doi:10.1016/j.neuint.2005.12.012
- Yu, G., Wang, L.-G., Han, Y., and He, Q.-Y. (2012). clusterProfiler: an R package for comparing biological themes among gene clusters. *OMICS* 16, 284–287. doi:10.1089/omi.2011.0118
- Zhang, X., Smits, A. H., van Tilburg, G. B., Ovaia, H., Huber, W., and Vermeulen, M. (2018). Proteome-wide identification of ubiquitin interactions using UbIA-MS. *Nat. Protoc.* 13, 530–550. doi:10.1038/nprot.2017.147
- Zhang, Y., Alexander, P. B., and Wang, X. F. (2017). TGF-beta family signaling in the control of cell proliferation and survival. *Cold Spring Harb. Perspect. Biol.* 9, a022145. doi:10.1101/cshperspect.a022145
- Zinda, M. J., Vlahos, C. J., and Lai, M. T. (2001). Ceramide induces the dephosphorylation and inhibition of constitutively activated akt in PTEN negative U87MG cells. *Biochem. Biophys. Res. Commun.* 280, 1107–1115. doi:10.1006/bbrc.2000.4248
- Zulato, E., Favaretto, F., Veronese, C., Campanaro, S., Marshall, J. D., Romano, S., et al. (2011). ALMS1-deficient fibroblasts over-express extra-cellular matrix components, display cell cycle delay and are resistant to apoptosis. *PLoS One* 6, e19081. doi:10.1371/journal.pone.0019081